Photoacoustic NeuroImaging

Darian Hadjiabadi and Timothy Mullen

May 8, 2015

Abstract

Current brain imaging techniques are insufficient to fully understand the action of neurons in the brain - exisiting techniques offer a steep tradeoff between temporal and spatial resolutions. Photoacoustic imaging is one imaging modality that may break this barrier. pH fluctuates in the outer layer of the neuronal body during action potentials, thus dyes sensitive to pH changes can have their photoacoustic outputs mueasured. The goal of this work is to provide insight on the photoacoustic output for a number of dyes along the 690-900 nm electromagnetic spectra, and to find the most appropriate for future studies by measuring the acoustic output while varying concentrations and pH. In addition, photoacoustic penetration was tested through introducing a bone phantom and subsequently varying its thickness. Results of this work show that concentration and pH variances can certainly effect the acoustic output, though the changes are somewhat obscure due to the number of variables at play. In particular, certain dyes may work better at lower concentrations, and certain dyes may have spectrum shifts at varying pH levels. Introducing the bone phantom changed the overall shape of the spectrum indicating the need for more research on the effects of acoustic output through a solid interface.

Introduction

Current brain imaging techniques are insufficient to fully understand the action of neurons in the brain. Existing techniques suffer a steep tradeoff between temporal and spatial resolution [4]. In 2014, The Johns Hopkins University and the University of Copenhagen won an NIH planning grant for Imaging In Vivo Neurotransmitter Modulation of Brain Network Activity in Realtime. [1]

Temporal resolution is the smallest time change at which an imaging modality can differentiate events. Action potentials (neural firings) usually take < 10 ms, so our imaging modalitys resolution must be in the order of milliseconds. PET, one of the best available brain imaging modalities, is far too slow, imaging activity in the order of minutes [4]. fMRI images more in real time, but only shows regions of activity that are nowhere close to the neuron level [4]. While the scans provided by PET and fMRI are useful, they dont tell the whole picture of how the brain operates. Neurons fire in an asynchronous signal cascade [8]. The signal begins at some neuron and propagates to different neurons as the event progresses. While these propagations often produce large amounts of activity in some region, the current regional imaging does not illustrate how the state of the response changes over time within the region [2]. Improving the spatial and temporal resolution of brain imaging is essential to progressing our understanding of brain function [3], and ultimately to developing and implementing therapies.

During action potential firing, neuronal pH levels rapidly fluctuate in the ranges of 5.5-7.5 [5]. pH sensitive dyes have been proven in vivo to respond to pH changes at the microsecond time scale [7][5]. Photoacoustic imaging allows the fluorescence change of the dyes to be measured through the skull, and through layers of tissue. Although the response of the dyes is the same, the photoacoustic system adds focused energy to magnify the response and transform it to mechanical waves that process better through the solid tissue.

The goal of this work is to develop noninvasive techniques for human brain imaging that provide good results in the millisecond time scale (the speed range in which neurons fire). The initiative aims to use intravenously delivered pH sensitive dyes that can indicate the firing of individual neurons in the brain, and to record the activity as signaled by the dyes. The hope is that photoacoustic imaging will allow noninvasive, fast, and accurate observance of signal changes, through the skull and layers of tissue.

In this paper we analyze the baseline photoacoustic spectra of various

dyes. In addition, the acoustic output is recorded across specific dyes of varying concentration and pH. While varying pH, a bone phantom is introduced for the purposes of gaining insight on the feasibility of the non-invasive nature of this imaging modality. Lastly, we measured the output across varying skull bone thicknesses. The rest of the paper is divided as follows: design, results, discussion, and concluding remarks.

Design

Our testing system consisted of four basic components: the dyes, a gel phantom containing a dye sample, the excitation laser, and a hydrophone to record the acoustic response.

Dyes

- Cyanine5.5 (Cy5.5)
- Aluminum 1,8,15,22-tetrakis(phenylthio)-29H,31H-phthalocyanine chloride (ALU-PHTH)
- Phthalocyanine Al(III) PcS-834 (Phtalocyanine)
- Alizirin-3-methyliminodiacetic acid (Alizirin)
- IR-780
- IR-783
- ICG 774.96
- 3,3-Diethylthiatricarbocyanine iodide
- Patent Blue V

These dye candidates were chosen due to their maximum absorption in the near infrared band. The near infrared spectrum theoretically allows for higher penetration into a sample [6]. From experiment, penetration depth in-vivo of the human breast was found to be approximately 40 mm using excitation wavelength 800 nm [3]. In controlled studies, this was further increased to 50-60 mm [3]. The human skull has an average thickness of 6

mm, thus in practice dyes located a few inches inside the brain will be able to be monitored for photoacoustic output.

Gel Phantom

To hold our dyes while testing, we designed a gelatin-based imaging phantom. Our final design consisted of a rectangular block of gelatin with a single, dome shaped fluid-holding well, protruding down from the top surface, into the block of gel. The laser beam is oriented perpendicular to one face of the gel, so that it intersects the dye in the well. The hydrophone, placed against the center of the wall, is 10 mm from the well. A mold was constructed that allowed four phantom blocks to be cast at a time, each with their own well.

The mold is constructed of 5 interlocking acrylic walls, and a lid that contains the cores that produce the wells. To cast, first the seams of the interlocking walls are sealed with cellophane tape. Hot water is mixed with powdered porcine gelatin until the solution is saturated. Undissolved powder and bubbles are skimmed off, and the liquid gelatin is allowed to degas in a hot water bath. The gelatin is then poured into the open topped mold and allowed to set until it has skinned. Once the gel has skinned, the lid is placed. The gel is allowed to cure for a minimum of 12 hours, and is used within 24 hours of casting. After curing, the lid can be carefully demolded, and the tape sealing the mold can be cut, allowing easy removal of the gel. The gel is then cut to separate the four phantom blocks, and the phantom blocks are ready to be used.

The gel design evolved through several iterations, and was optimized for use with our photoacoustic system. We had originally planned to align the laser and hydrophone opposite each other, with the gel and well in between, and our first phantom was constructed to accommodate this. However, when we tried to use this setup, we found that the light that transmitted through the well and struck the hydrophone caused excessive noise and obscured the photoacoustic response of the dye. The gel was redesigned to function in a perpendicular orientation, with the wells repositioned as per the final design to preserve homogeneity along the laser/acoustic paths, as well as consistent distances for each well.

OPO Laser System

The Optical Parametric Oscillator (OPO) laser system provided the light energy necessary for photoacoustic response. An input (1) pump frequency is separated into its signal (2) and idler (3) components such that the frequency sum of (2) and (3) equals the frequency of (1) - a trivial consequence of the conservation of energy. It is convention to correspond the higher frequency wave as the signal wave.

The OPO laser consists of a nonlinear optical crystal which serves to amplify the signal and idle waves while subsequently deamplifying the pump wave. The gain of the idle and signal waves allows for one or both to resonate in an optical resonator. The frequency of the output waves can be controlled by changing the frequency of the pump wave, which was done so through provided software. The OPO system allows any wavelength within a continuum to be selected, and does not lock the user into a fixed number of wavelengths or step size.

Our project involved bombarding the dyes housed in the gel phantom well with light in the 690-900 nm range for reasons mentioned in the discussion of dyes. An interface box connected the laser with the software needed to fine tune the output wavelength. The output light was controlled using a mirror system that had to be manually tuned in order to directly impact the well. Using a fiber optic cable was initially suggested due to its flexibility in bombarding the dye from all spatial dimensions. However, due to a malfunction in the fiber optic cable, the mirror system was used as our testing standard.

Hydrophone

A hydrophone behaves like a microphone, turning acoustic waves into a voltage output, except hydrophones are optimized to respond to acoustic waves in water as opposed to air. An Onda HGL series hydrophone with AH-2020 preamp was chosen for its high sensitivity and flat response over a large band. While many other photoacoustic studies use ultrasound probes to measure the acoustic signal, we desired the hydrophones sensitivity, given we did not know what magnitude of response to expect from our dye candidates. Again, in the interest of accuracy and sensitivity, we recorded the hydrophone output with an oscilloscope as opposed to using a faster, automated DAQ known to produce lower quality readings. Pictures of our setup can be found in Supplementary section. In addition, the supplementary material shows what the

photoacoustic wave looks like and how to acquire the output.

Results

This section will comprise of data obtained through experiment. Explanations will be provided in the Discussion.

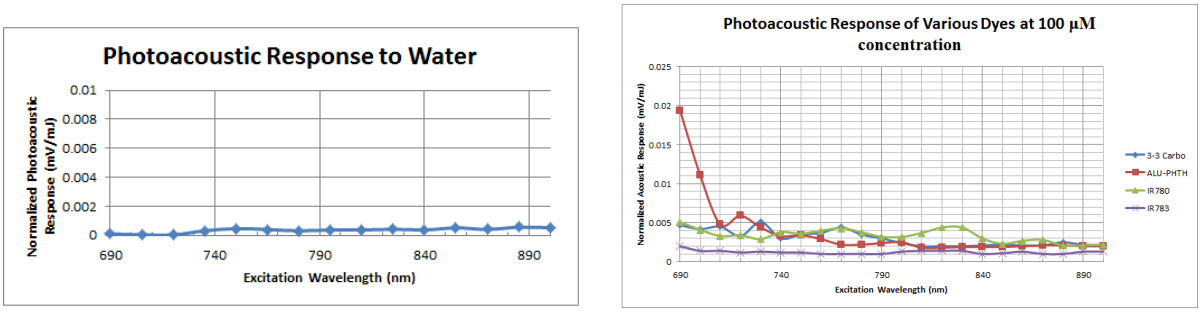

Figure 1: Baseline readings for water and various dyes

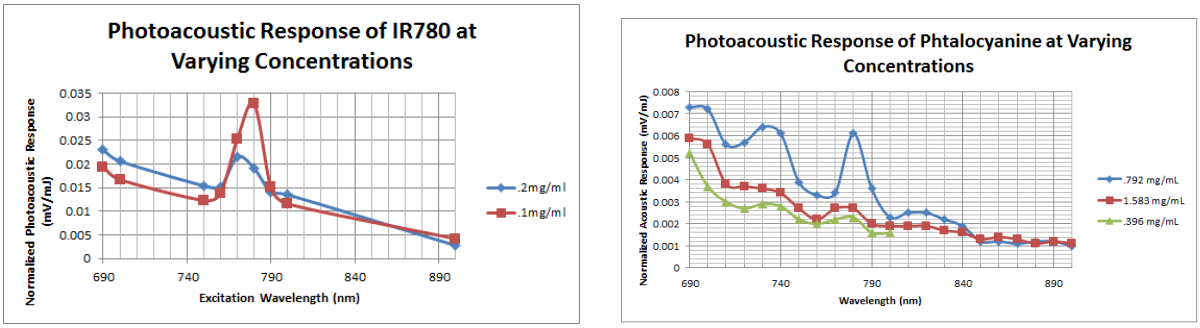

Figure 2: Changing concentration

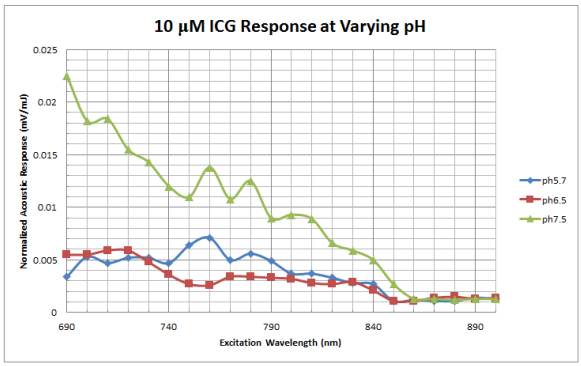

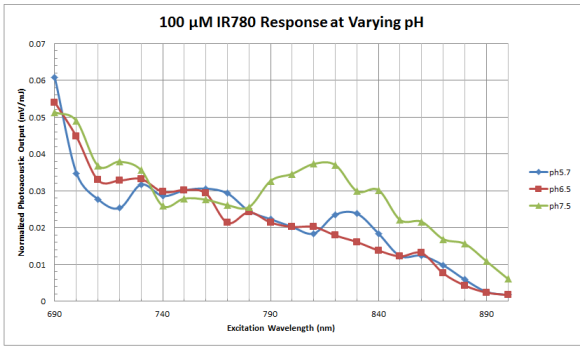

Figure 3: Changing pH

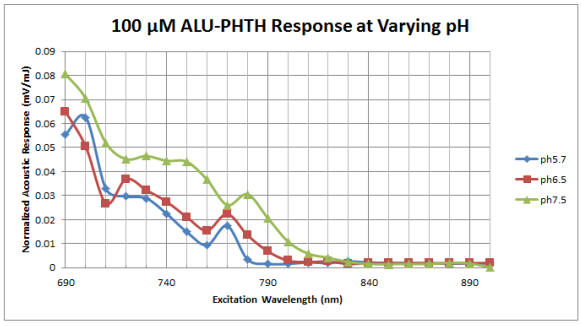

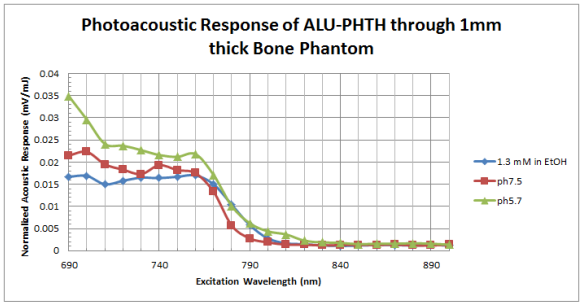

Figure 4: Changing pH and introducing skull bone

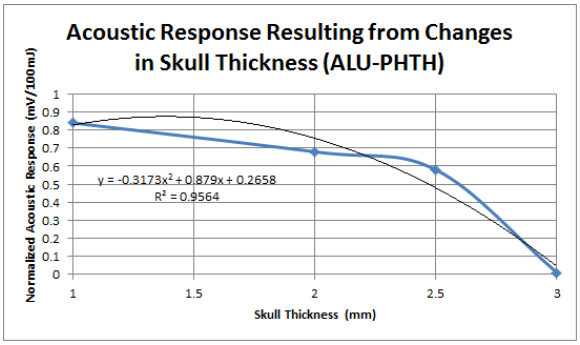

Figure 5: Varying skull bone thickness

Discussion

Figure 1 left shows the baseline reading of water. The results are what one would expect - flat. It was necessary to take this reading in order to differentiate photoacoustic ouput from noise. Figure 1 right gives the baseline acoustic response for a number of dyes. ALU-PHTH had a much higher response in the early wavelength range, making it a possible candidate dye for further testing. On the other extreme, IR-783 recorded a very flat response. IR-780 and 33-Carbo fell inbetween.

Figure 2 left and right show how varying concentration effect the photoacoustic output for IR-780 and Phtalocyanine, respectively. The left graph, IR-780, had maximum photoacoustic output at 780 nm as the name of the dye alludes to. What is interesting to note is that the peak was higher at the lower concentration then the higher concentration. This may be a result of the photobleaching effect, however it should be noted that there are several more obscure variables at work that may lead to this result. Regardless, this certainly gives the impression that too much of something may not necessarily work in one's favor. The right graph also supports this rather cliche statement. Note that at .792 mg/ml, the response was higher than at 1.583 mg/ml. In addition, the outputs accross the three measured concentrations followed similiar shapes with the higher response producing more intense peaks - this general trend gives confidence in the output. .396 mg/ml gave the weakest output, suggesting there is an upper and lower bound to which concentrations lying within this bound will produce the optimal and more intense photoacoustic outputs.

Figure 3 gives the pH trend for ICG (left) and IR780 (right). The highest response for ICG was observed at pH 7.5 while 6.5 and 5.7 pH levels had similiar outputs. ICG observed significant shift when varying the pH at 7.5, 6.5, and 5.7. At pH 7.5, maximum output was recorded at the 690nm excitation wavelength. At 6.5, this was recorded at the 720nm nanometer wavelength. At 5.7 pH, this was recorded at the 760 nm wavelength. This shift provides crucial information on the behavior of dyes during neuronal action potentials. In particular, this is useful for providing an "ON", "OFF" characteristic. If a neuron holds a particular pH before firing, and the dye surrounding this neuron has a maximum response at that pH, then on firing this response will almost immediately fall. IR780 provided an unusual result in that the maximum acoustic response was found at 690nm across all three pH levels. There is a possibility of experimental error in this instance.

Figure 4 compares ALU-PHTH across pH levels (left) and further studies the response through introduction of a skull bone (right). ALU-PHTH was chosen in this instance as it had the highest response in Figure 1 right. Figure 4 left shows that response increases with increasing pH. In addition, one interesting result from this experiment is that the 770nm local maximumum at pH 5.7 and 6.5 turned into a local minima for pH 7.5. In fact, at this excitation wavelength in particular, the response at all three pH levels converged to a particular acoustic output value. The surrounding neighborhood at excitation wavelength 770nm for pH 5.7 and 6.5 were lower than this point and thus explains the local maximum. Likewise, the neighborhood of 770nm for pH 7.5 were greater than this point and thus explains the local minimum. However, it not clear why in particular the response across the pH board converged in the first place. In Figure 4 right, response was measured after putting a 1mm thick skull bone in front of the hydrophone. Results show a smoothing effect taking place in that the local maximum and minimum at 770 nm for the three pH values are essentially lost. While this is not necessary a positive result, it is important to understand the effects of the skull bone on photoacoustic output as the aim is to provide neuron information in real time without compromising the skull. Also of interest is why at pH 5.7 the output is largest in the 690-770 nm band. Again, this may be a result of experimental error or could be a direct result of putting a solid material in front of the hydrophone. Unfortunately, we did not have enough time to run more tests, so further research will aim to repeat this experiment.

Figure 5 put recorded acoustic response of ALU-PHTH to varying bone thicknesses. Results show a quadratic decay which is supported by the reading material [2]. That is, doubling the thickness decreases the response 4x.

Conclusion

Photoacoustic imaging of fluorescent dyes may break through the current barrier of imaging neuronal activity in real time. This study aimed to give future researchers a first hand look at the photoacoustic output for an assortment of dyes, and to study the effects of varying concentration and pH. Future research would focus on repeating tests that we started in this work in order to confirm the trends observed. In addition, delving deeper into finding the reasons for particular phenomenon, such as the convergence seen in figure 4 left and the smoothing in figure 4 right, will be useful in predicting

the behavior of other dyes. We would like to thank our mentor Dr Emad Boctor for introducing us to photoacoustic imaging and for allowing us to participate in the early stages of the NIH BRAIN initiative. We would also like to thank Dr Behnoosh Takavoli for spending hours with us in the lab training us and for helping our research go by more smoothly. We could not have done it without you. Furthermore, thanks to Dr Daniel Thorek and Dr Julie Pickett for helping us pick out dyes and acquiring buffer solutions.

References

[1] The brain iniative. http://www.braininiative.nih.gov/funding.htm, 2015.

[2] Paul Beard. Biomedical photoacoustic imaging.

[3] Emad Boctor and Nathanel Kuo. Photoacoustic imaging of prostate brachytherapy seeds in ex vivo prostate.

[4] Cox B.T., Laufer J.G., and Beard P.C. The challenges of quantative photoacoustic imaging.

[5] Muhammad Chatni, Junji Yao, and Amos Danielli. Functional photoacoustic microscopy of ph.

[6] Treger Jeremy and Michael Priest. Real-time imaging of electric signals with an infrared fda-approved dye.

[7] Jetena Levi, Ma Ta-Jea, and Keth Hartman. Design, synthesis, and imaging of an activatable photoacoustic probe.

[8] Per Roland, Eriksson David, and Tompa Tomas. Non-linear population firing rates and voltage sensitive dye signals in visual areas 17 and 18 to short duration stimuli.

1 Supplementary

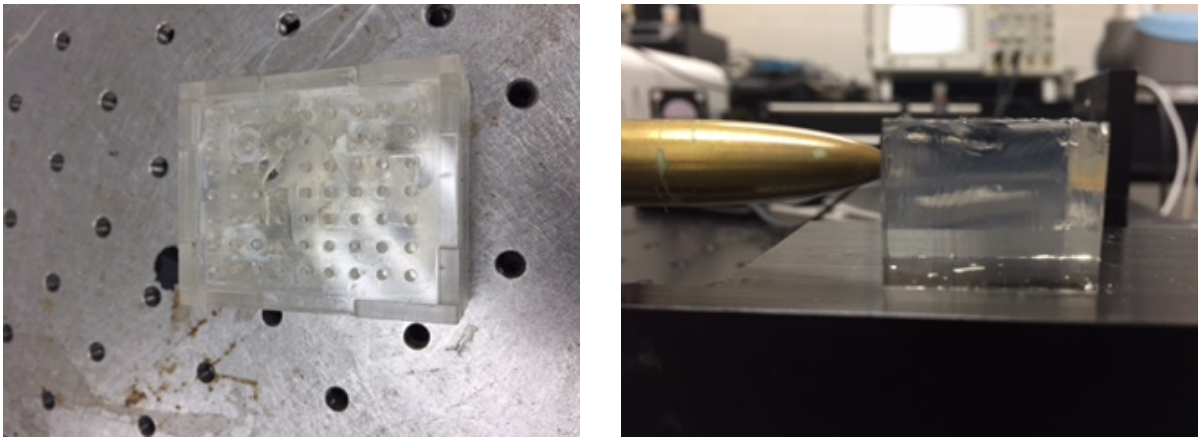

Figure 5: Left: Gel phantom in acrylic box. Right: hydrophone making contact with gel

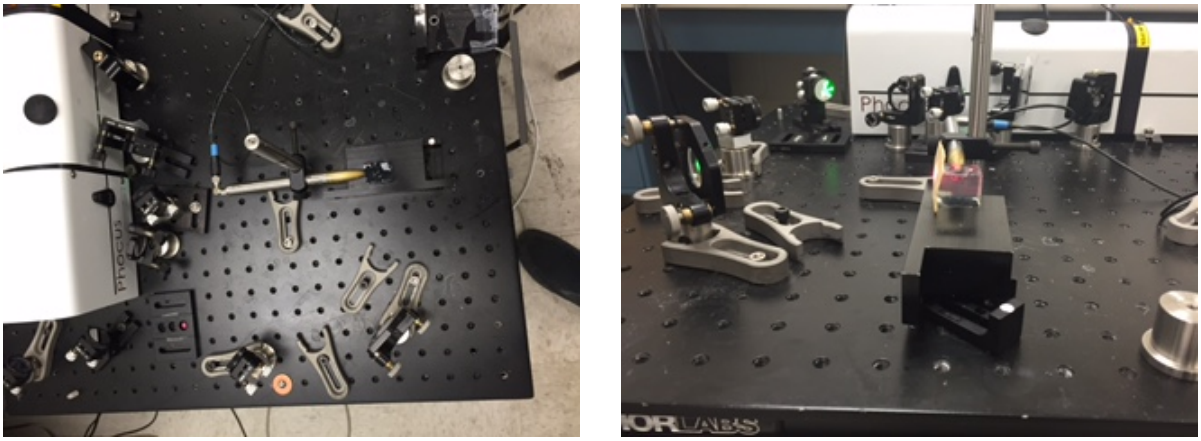

Figure 6: Left: Top view of our setup. Right: Setup in action with skull bone in front of hydrophone

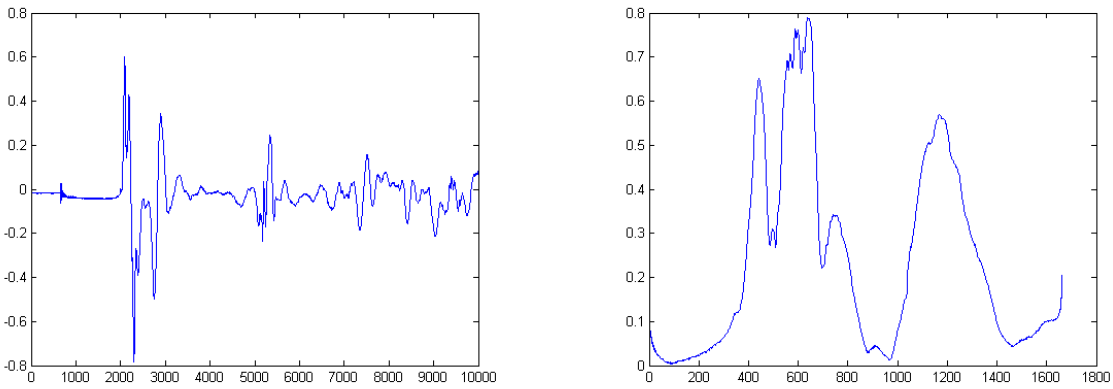

Figure 7: Left: Photoacoustic wave can be seen along the interval [2000,4000] of the x-axis. Right: Envelope after Hilbert transform. Photoacoustic output is determined by the suprenum of this graph.